Introduction to the Workshop

Marvin A. Geller
Stony Brook University
Stony Brook, New York USA
Marvin.Geller@sunysb.edu

This workshop is sponsored by the FISAPS (Fine-Scale Atmospheric Processes and Structures) activity of SPARC (Stratosphere-troposphere Processes And their Role in Climate). SPARC is a core project of the WCRP (World Climate Research Programme).

This workshop is sponsored by the FISAPS (Fine-Scale Atmospheric Processes and Structures) of SPARC (Stratosphere-troposphere Processes and their Role in Climate). SPARC is a core project of the WCRP (World Climate Research Programme).

There will be an acronym exam at the end of the workshop.

The goals of FISAPS are as follows.

1. Stimulate research on fine-scale atmospheric processes and structures that are important for global modeling and other societal benefits.
2. Increase access to global High Vertical-Resolution Radiosonde Data (HVRRD).

The focus of this workshop will be on new research results using available global HVRRD. More limited regional data have been widely used for studies of gravity waves, turbulence, tropopause structure, and planetary boundary layer depths. There will also be discussions on using these data together with GPS occultation and aircraft data.

SPARC became a core project of the WCRP in 1992.

In 1993, one of SPARC’s first nine activities was “Gravity Wave Processes and Parameterization” with Robert Vincent and Kevin Hamilton as activity co-chairs.

JOURNAL OF GEOPHYSICAL RESEARCH, VOL. 100, NO. D1, PAGES 1327–1350, JANUARY 20, 1995

Gravity wave activity in the lower atmosphere: Seasonal and latitudinal variations

Simon J. Allen and Robert A. Vincent
Department of Physics and Mathematical Physics, University of Adelaide, Adelaide, South Australia

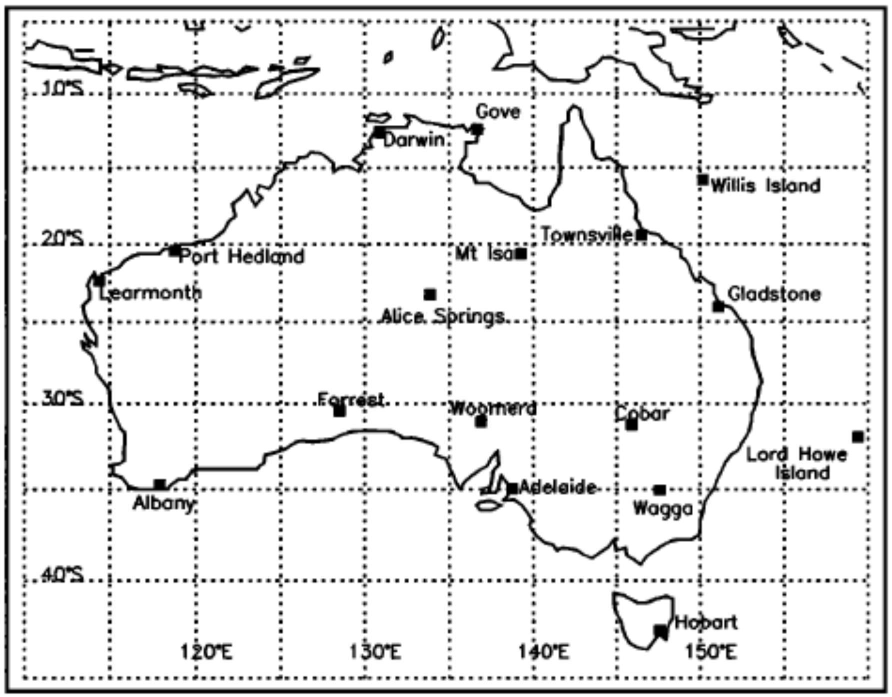

Figure 1. The geographic distribution of radiosonde stations used in the study. Davis (69°S, 78°E), in Antarctica, is not shown.

Used HVRRD temperatures taken every 10 seconds, implying 50 m vertical resolution

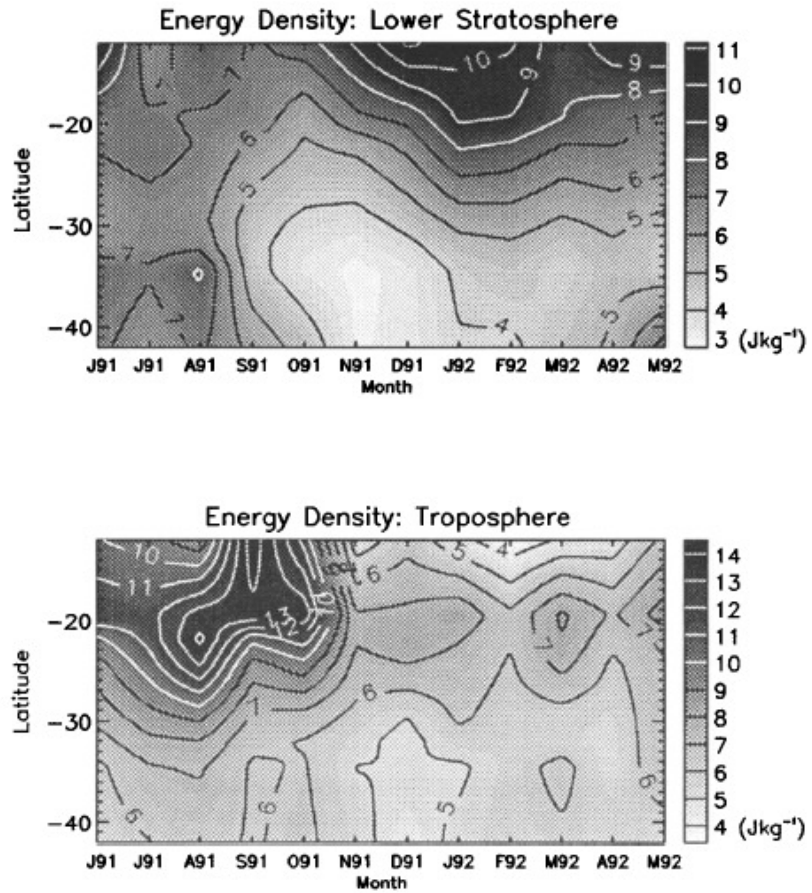

Figure 7. Time-latitude contours of total gravity wave energy density, E_0, for the troposphere and lower stratosphere. The energy density is calculated using (6) where $\overline{\hat{T}'^2}$ is the normalized temperature variance within the height intervals described in Table 1.

Troposphere
~2-9 km

Lower Stratosphere
~17-24 km

Eos, Vol. 76, No. 49, December 5, 1995

EOS, TRANSACTIONS, AMERICAN GEOPHYSICAL UNION

EOS

VOLUME 75 NUMBER 49

DECEMBER 5, 1995

PAGES 609–616

High-Resolution Radiosonde Data Offer New Prospects for Research

PAGES 497, 506–407

Kevin Hamilton and Robert A. Vincent

Determination of Gravity Wave Characteristics

High-resolution radiosonde observations can be exploited to study gravity waves. *Allen and Vincent* [1995] used high-resolution radiosonde temperature data from 18 stations in the ABM network to investigate gravity wave activity in the troposphere and lower stratosphere. They considered the effects of sensor lag on the temperature soundings and

In 2000, I received an NSF grant that enabled me to purchase HVRRD from NOAA, and a NASA grant that allowed me to set up the SPARC Data Center to disseminate those, and other, data.

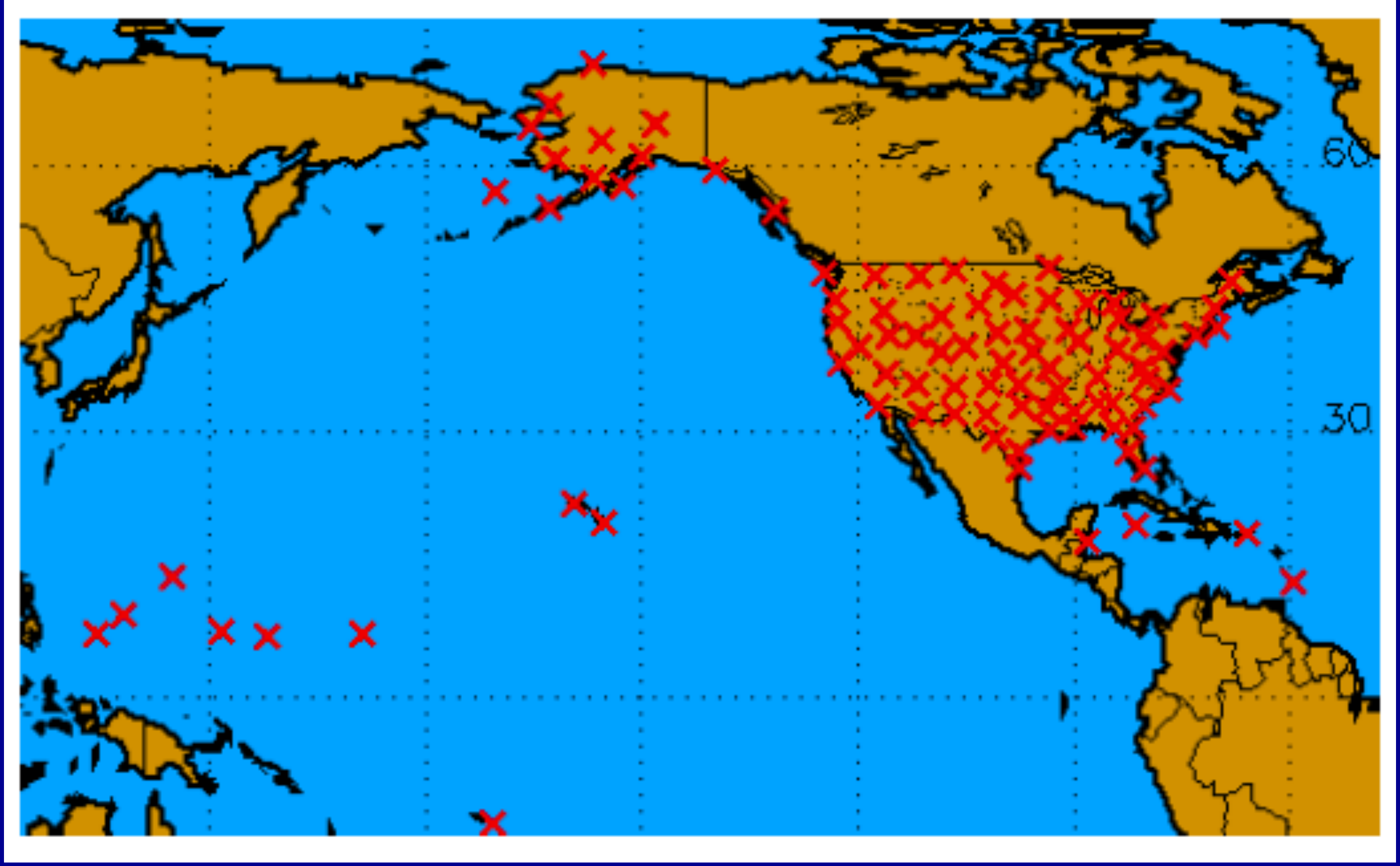

This US HVRRD initially were 6-s data, but later transitioned to 1-s data as GPS radiosondes were introduced.

Total GW Energy Density (kinetic plus potential)

Troposphere (2-9 km)

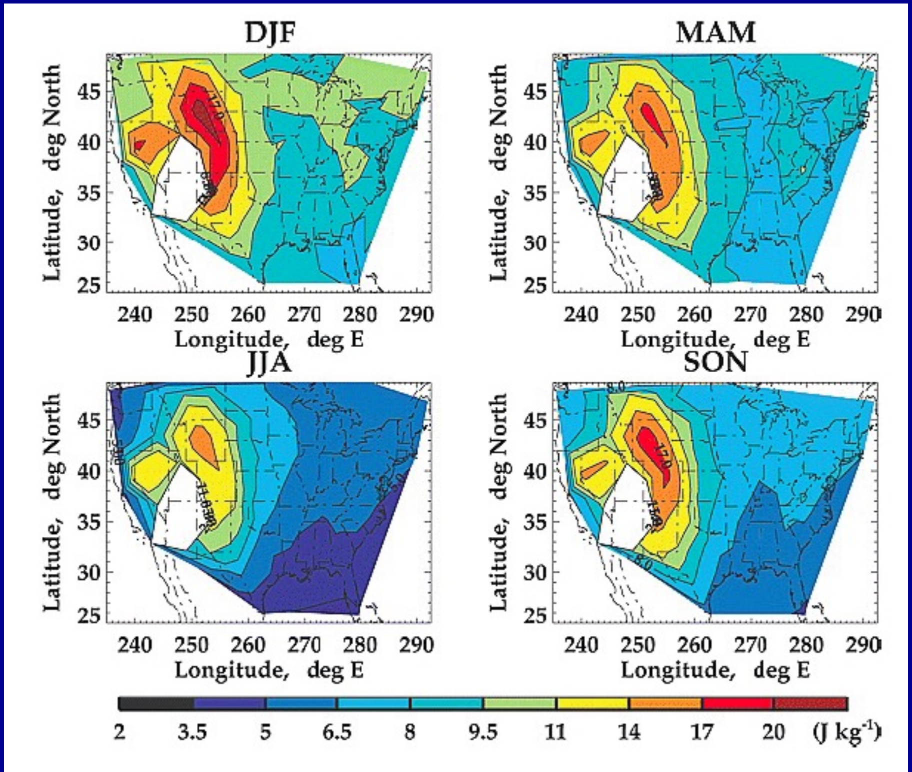

Lower Stratosphere (17-24 km)

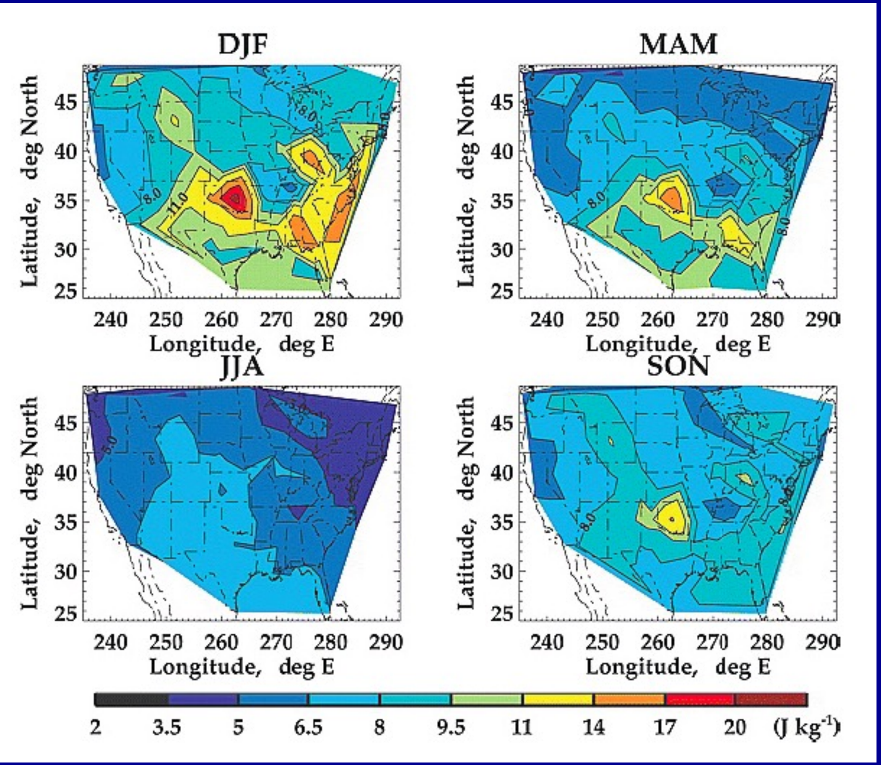

From Wang and Geller (2003, JGR)

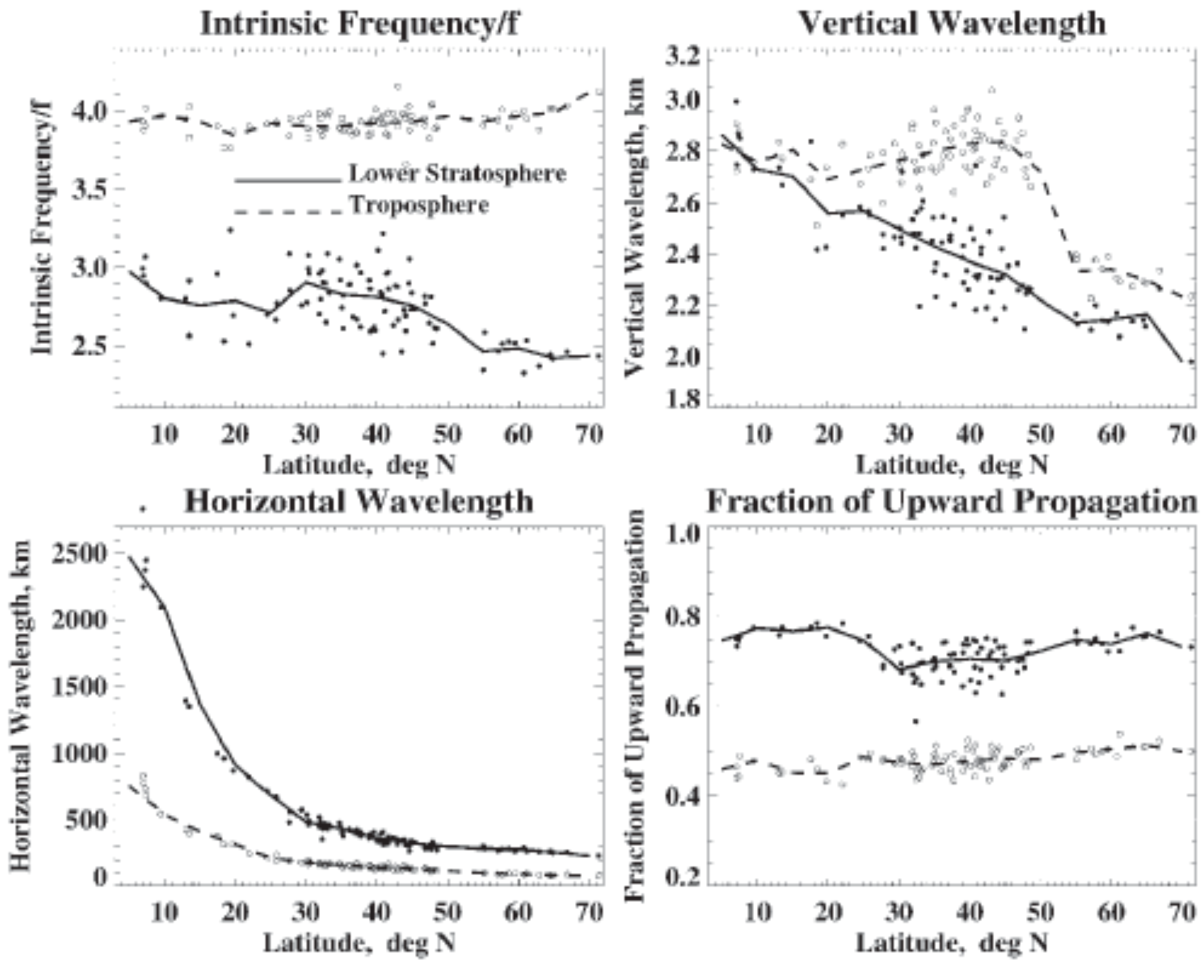

FIG. 6. Five-year (1998–2002), averaged $\hat{\omega}/f$, $\overline{\lambda}_z$, $\overline{\lambda}_h$, and fractions of upward propagation as functions of latitude in the troposphere (open dots) and lower stratosphere (filled dots). The dashed and solid lines are the latitudinal binned results (with a bin size of 5°) for the troposphere and lower stratosphere, respectively.

From Wang, Geller, and Alexander (2005, JGR)

Tropopause Structure

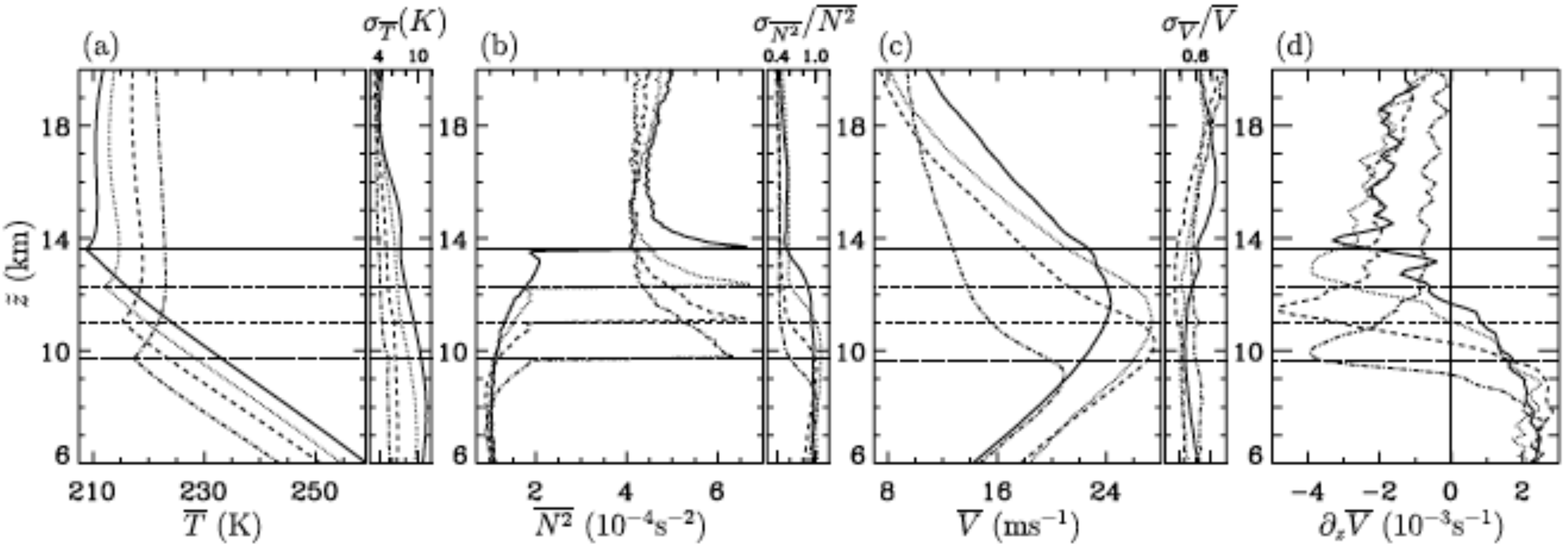

Figure 3. Annual TB climatologies and corresponding standard deviations (σ) of (a) temperature, (b) buoyancy frequency squared, (c) horizontal wind, and (d) vertical shear of the horizontal wind of the four stations: Miramar NAS, California (33°N, 117°W, solid); Reno, Nevada (40°N, 120°W, dotted); Quillayute, Washington (48°N, 125°W, dashed); and Yakutat, Alaska (60°N, 140°W, dash-dotted). Horizontal lines denote $\overline{z_{TP}}$.

From Birner (2006, JGR)

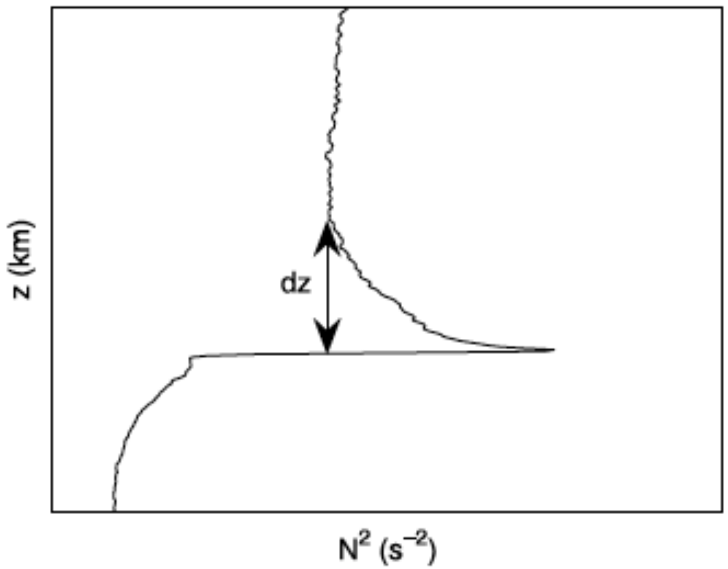

Figure 2. Schematic showing approximate depth of ESTL.

From Bell and Geller (2008)

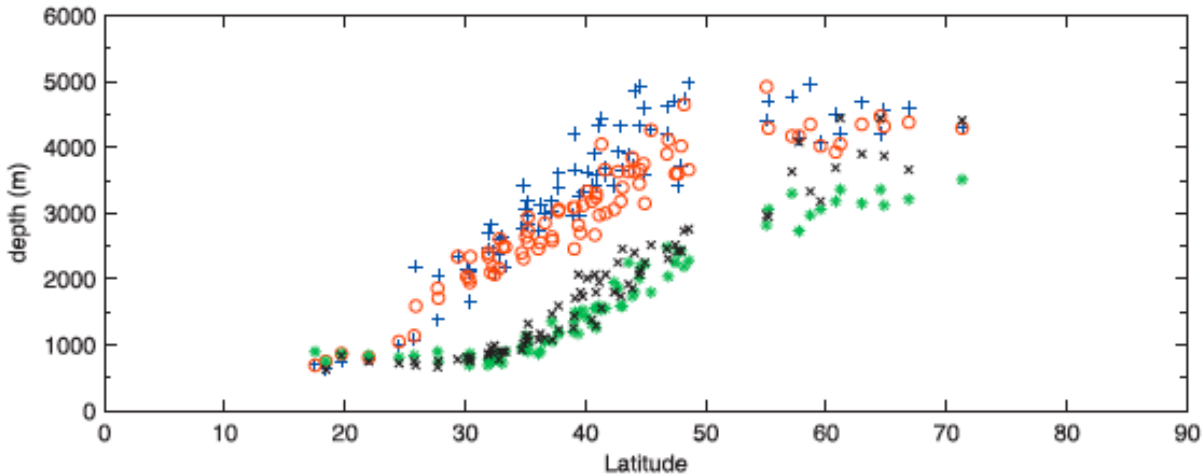

Figure 4. Seasonally averaged latitudinal variability of the ESTL depth for high-resolution data for DJF (blue pluses), MAM (red circles), JJA (green asterisks) and SON (black crosses).

Vertical Velocity Fluctuations

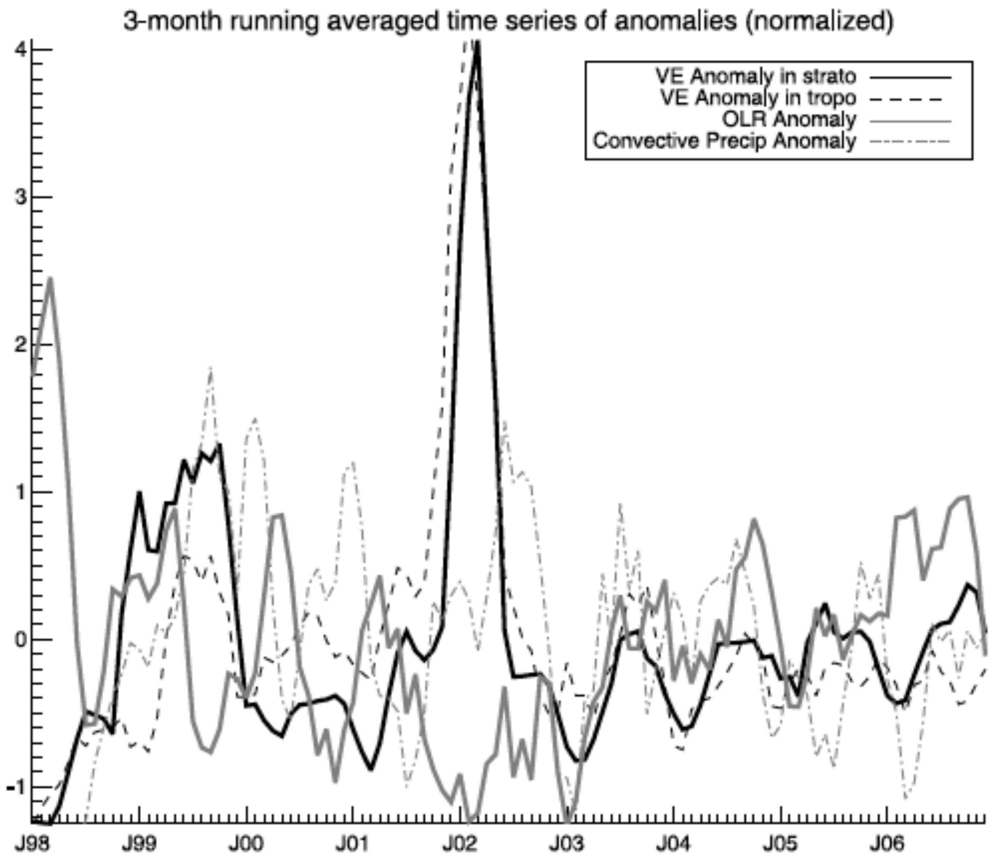

Figure 2. Normalized monthly mean of anomalies of VE in lower stratosphere (black solid), troposphere (black dashed), OLR (gray solid), and convective precipitation at the surface (gray dash-dotted) over Majuro/Marshall Island [171.38°E, 7.08°N]. A 3-month running window has been applied to the time series.

VE_{trop} : VE_{strat} r = 0.813

VE_{trop} : OLR r = -0.513

VE_{strat} : OLR r = -0.358

VE_{trop} : CPR r = 0.291

Ve_{strat} : CPR r = 0.330

From Gong and Geller (2010)

Boundary Layer Depths

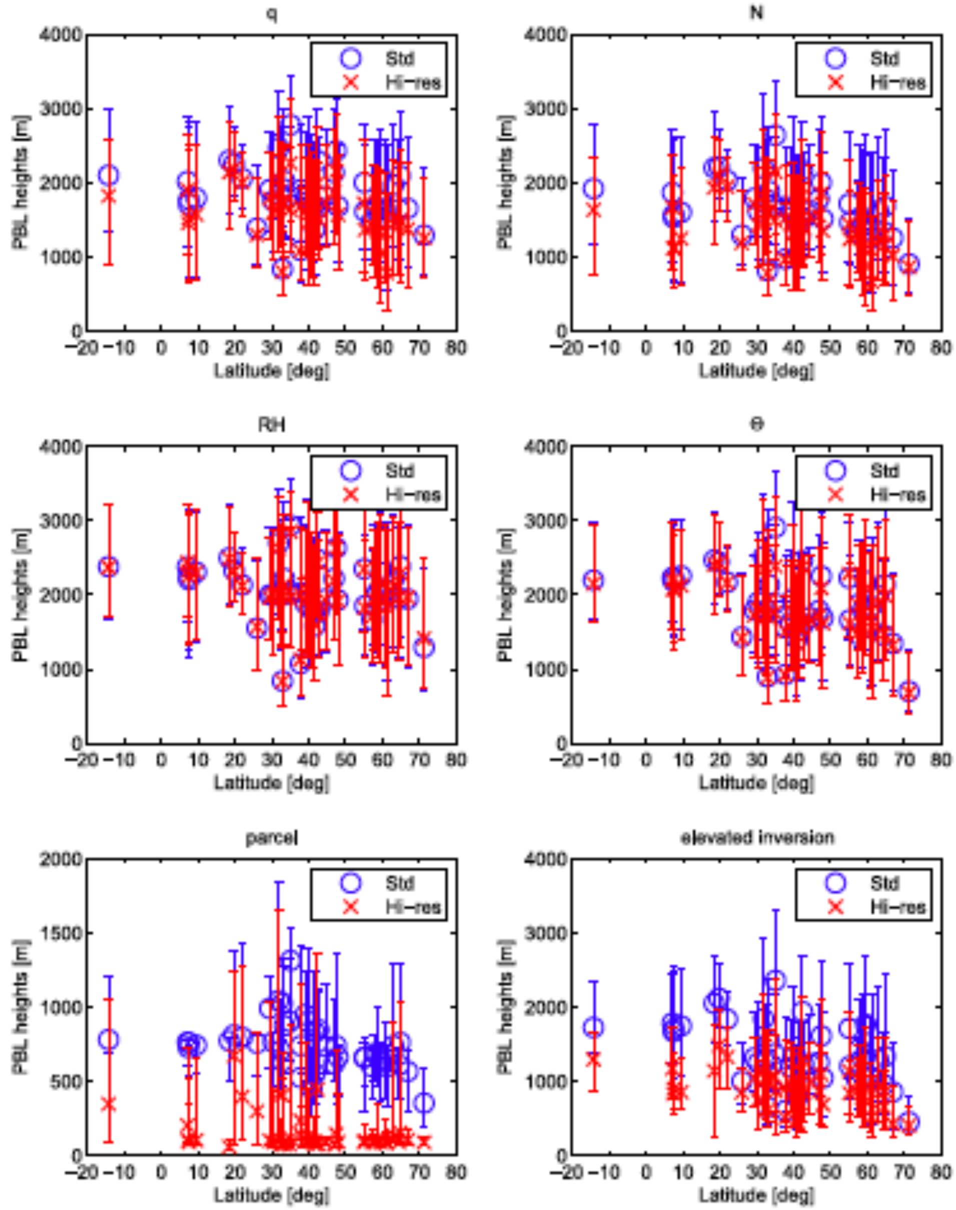

Figure 10. Comparison of 25th, 50th and 75th percentile values of PBL heights (m) from 44 stations based on standard (blue) and high (red) vertical resolution sounding data, as a function of station latitude. Each frame shows results for a different method of estimating PBL height using observations for 1999–2007. Note the different vertical axis scale for the parcel method (lower left frame).

From Seidel, Ao, and Li (2010, JGR)

Turbulence

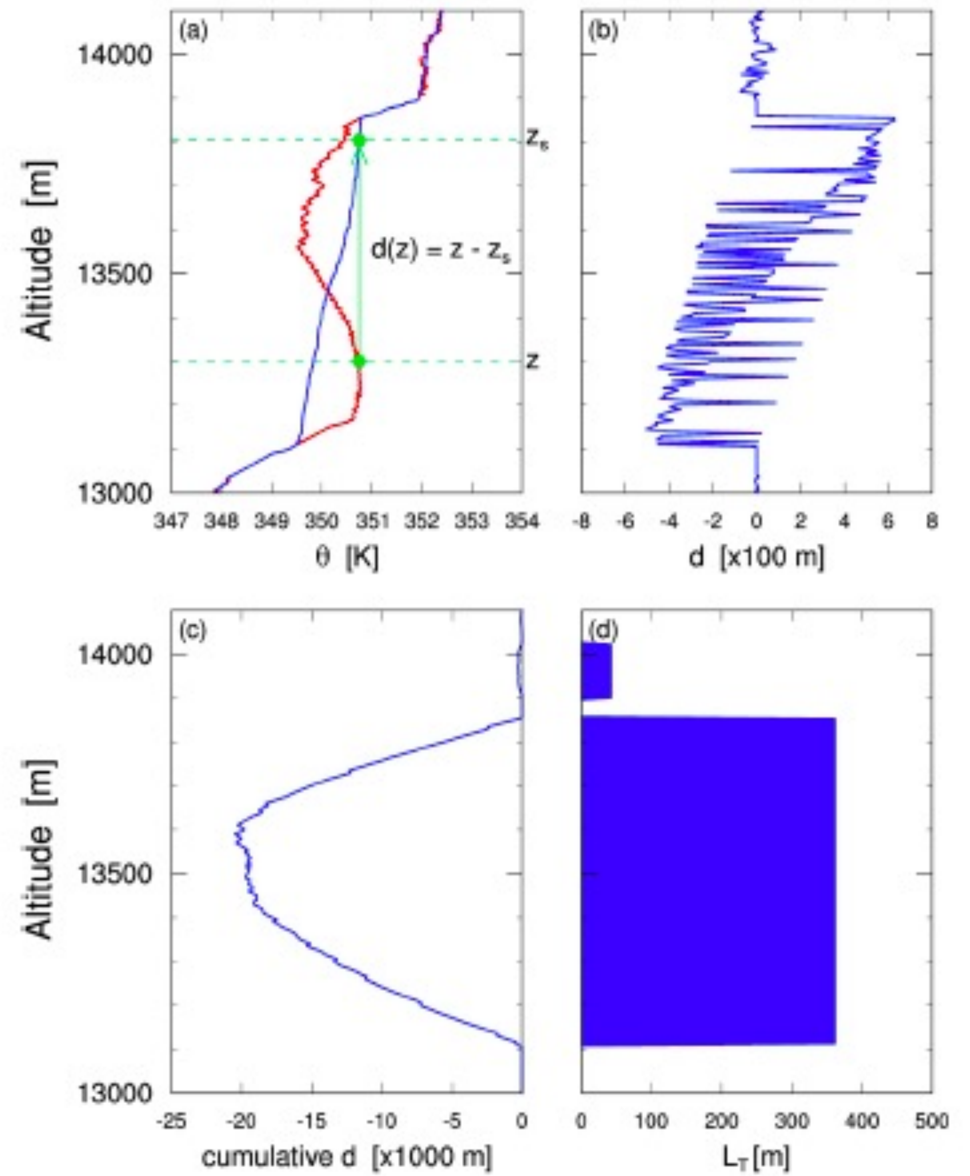

Figure 3. The Thorpe analysis process. (a) Observed (red) and re-sorted (blue) profiles of reconstructed potential temperature, (b) Thorpe displacement, (c) cumulative Thorpe displacement, and (d) Thorpe scale.

Illustration of the Thorpe method (Thorpe, 1977) applied to the atmosphere, as suggested by Clayson and Kantha (2008)

Taken from Ko et al. (2019)

$\varepsilon = N^3 L_O^2$, where It is assumed that $L_O = cL_T$

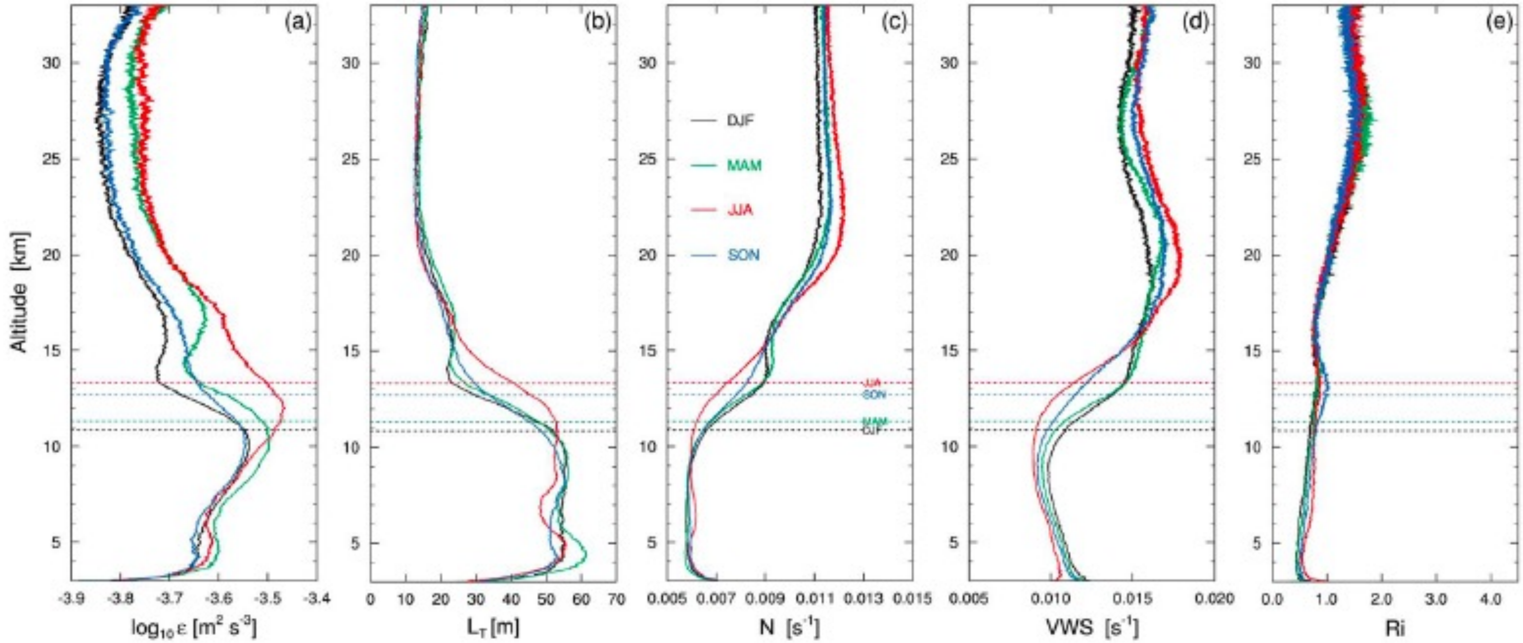

Figure 7. Vertical profiles of the seasonal mean of (a) logarithmic eddy dissipation rate ($\log_{10}\varepsilon$), (b) Thorpe scale (L_T), (c) Brunt-Väisälä frequency (N), (d) vertical wind shear, and (e) gradient Richardson number (Ri) for 4 years (September 2012 to August 2016). The seasonal mean tropopause height is represented by the horizontal dashed line in each plot. Note that only the N, vertical wind shear, and Ri within turbulent layers are used in (c), (d), and (e), respectively. Turbulent layers containing $z = 3$ km are not used in calculating each mean profile. DJF = December–February; JJA = June–August; MAM = March–May; SON = September–November.

From Ko et al. (2019)

Using HVRRD as a Transfer Standard

Two Examples

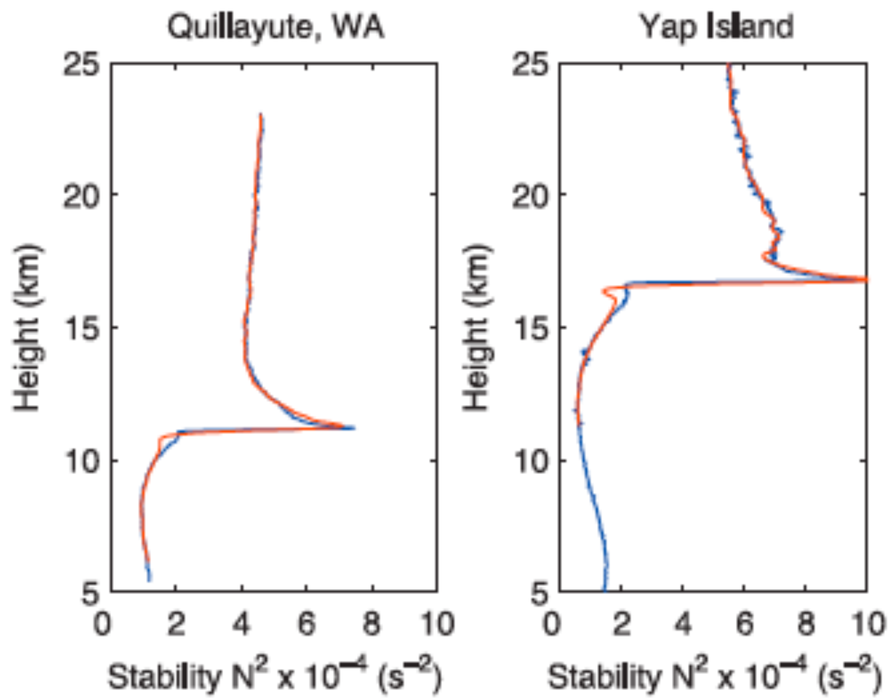

Figure 5. Stability profiles derived from standard data (red) and high-resolution data (blue, solid lines) for (left) Quillayute, WA, and (right) Yap Island.

From Bell and Geller (2008, JGR)

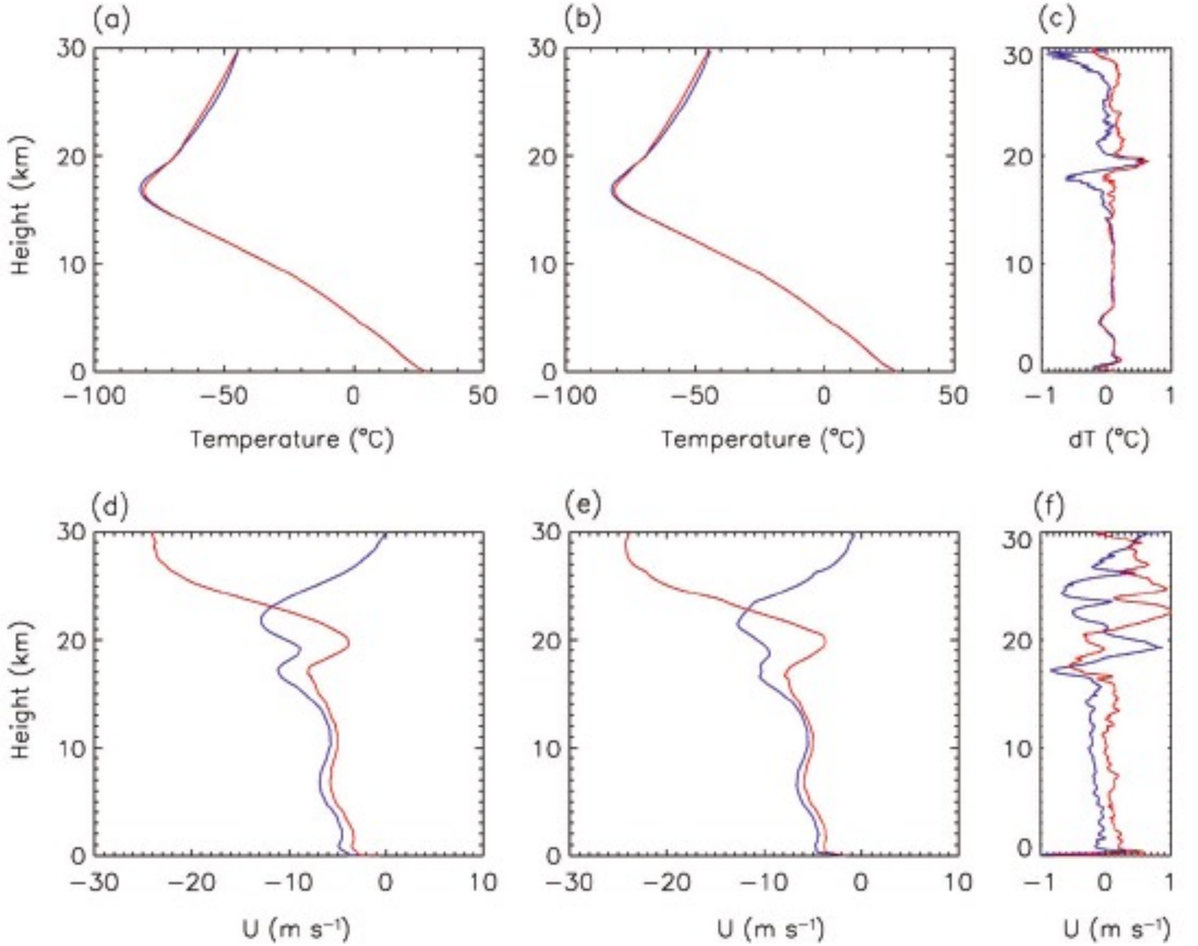

Figure 1. Comparison of composite QBO easterly (blue) and westerly (red) temperature profiles (top) and zonal wind profiles (bottom) using high vertical-resolution radiosonde data (left) and IGRA data (middle) for the years 1998–2008 at Yap Island (9.48°N, 138.08°E). The right column shows (c) the temperature and (f) zonal wind differences between HRES/IGRA: blue is during the QBO easterly phase whereas red is during the QBO westerly phase. The data were composited using a 6 month phase lag according to the wind shear at 50 hPa. The units of zonal wind and temperature are m s^{-1} and °C.

From Yuan, Geller, and Love (2014, QJRMS)

Increased HVRRD Availability

Allen and Vincent (1995)

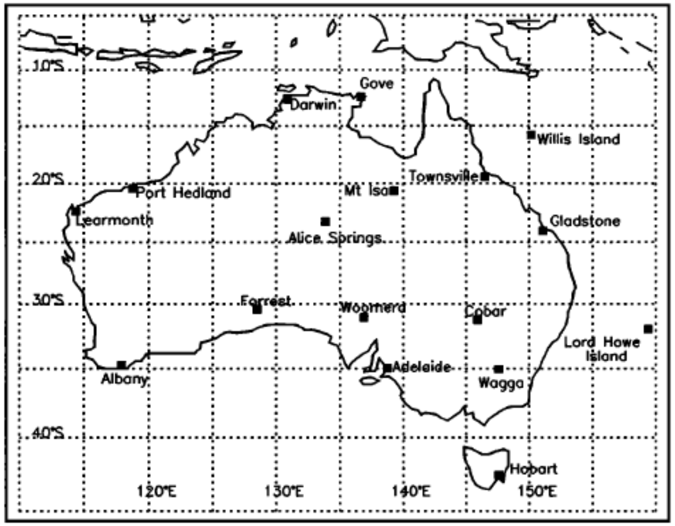

Figure 1. The geographic distribution of radiosonde stations used in the study. Davis (69°S, 78°E), in Antarctica, is not shown.

->

Wang and Geller (2003)

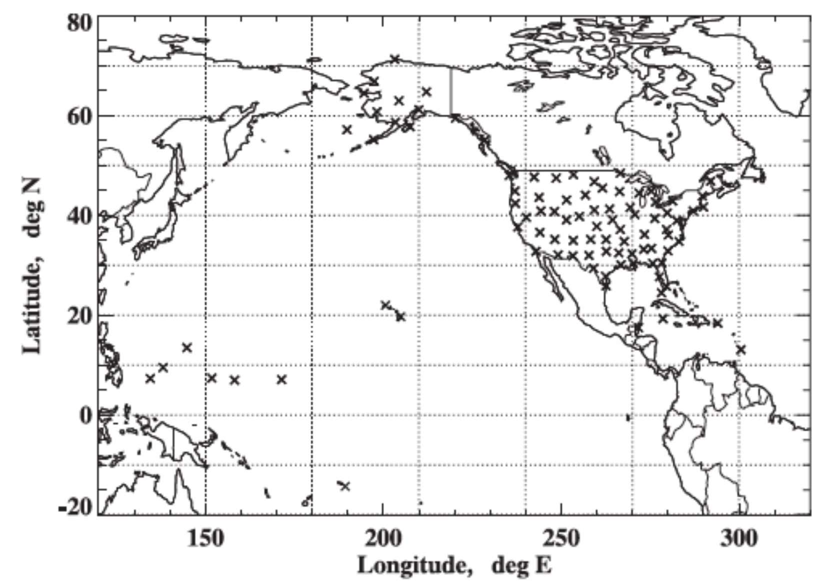

->

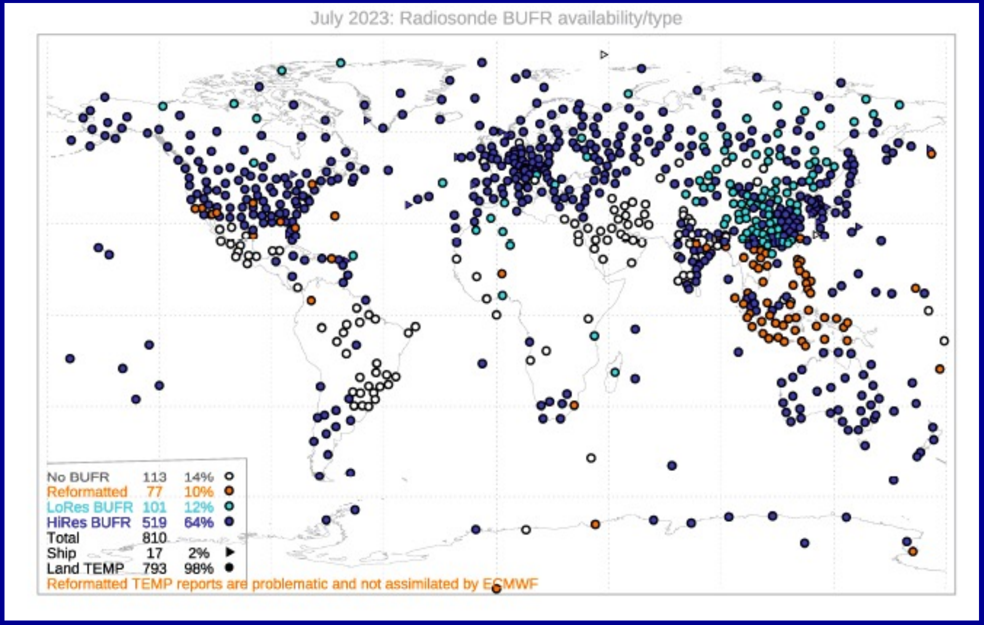

From Bruce Ingleby's talk later in the workshop